Letters in Applied NanoBioScience
Open-Access Journal (ISSN: 2284-6808)

Article
Volume 12, Issue 2, 2023, 47
https://doi.org/10.33263/LIANBS122.047

Optical and Structural Studies of Tin Disulfide (SnS_2) Synthesized by Facile Hydrothermal Method

Nipom Sekhar Das [1], Asim Roy [1], Avijit Chowdhury [1,2*]

[1] Department of Physics, National Institute of Technology Silchar, Silchar, Assam-788010, India
[2] Department of Condensed Matter Physics and Material Sciences, S. N. Bose National Centre for Basic Sciences, JD Block, Sector-III, Salt Lake, Kolkata-700106, West Bengal, India
* Correspondence: avijitiacs@gmail.com (A.C.);

Scopus Author ID 57196117274
Received: 11.01.2022; Accepted: 5.02.2022; Published: 19.03.2022

Abstract: Transition metal dichalcogenides (TMDCs) have found diverse applications for intrinsic semiconducting and tunable electronic properties mediated via the van der Waals interaction between the adjacent chalcogen planes. Therefore, the large-scale production of TMDCs without compromising the material properties is the major challenge at the present moment. We follow a simple, cost-effective, and environmentally friendly hydrothermal technique for synthesizing tin disulfide (SnS_2). The optical properties are investigated using UV-visible, photoluminescence (PL), Raman, and FTIR spectroscopy. The UV-visible absorption spectra of pure SnS_2 show a broad absorption peak located at 340 nm, and the corresponding optical band gap energies are estimated to be 2.14 and 4.02 eV, respectively. The PL spectra display a sharp emission peak at 561 nm due to the radiative recombination of bound excitons for the excitation wavelength of 340 nm. FTIR is used to observe the existence of functional groups in the material. The absorption peak observes at 625 cm^{-1} corresponds to the vibration of the Sn-S bond. From Raman spectra, a sharp peak appears at 314 $cm^{-1,}$ corresponding to the A1g mode of pure SnS2, which occurs due to the out-of-plane stretching vibration of sulfur atoms in the SnS_2 material. The XRD is used to identify structural phases. The sharp diffraction peaks at $2\Theta = 15.17^{O}$ and 28.55^{O} corresponds to (001) and (100) planes, respectively, that suggest the hexagonal phase of pure SnS_2. Interplanar spacing is estimated using Bragg's law, and the value is found to be 5.83 Å. The average crystallite size is estimated to be 28 nm from the Williamson-Hall plot, which is comparable with the crystallite size calculated from Scherrer's formula.

Keywords: tin disulfide; hydrothermal; band-gap; Tauc's plot.

1. Introduction

The layered semiconducting materials transition metal dichalcogenides (TMDCs) are well-known for their fascinating electronic and optoelectronic characteristics, sizeable and tunable band-gap, and high in-plane carrier mobility [1,2]. Therefore, understanding the optical and electronic properties of TMDCs originated from their structural confinement is crucial from a technological and device application perspective [3-5]. Among the different TMDCs, tin disulfide (SnS_2) has drawn promising interest because of its superb electronic and optical properties [6-10]. The SnS_2 is a layered n-type semiconducting material having a band gap in the range between 2-3 eV [1,11], which makes it a promising candidate for various exploitations such as solar cells, optoelectronic devices, and lithium cells, sodium ion storage, sensors, nano semiconductor devices, etc. [12-24]. The band-gap energy of the nanomaterials

depends on the number of layers. Hence, the electronic properties can be tuned easily through precise control. The structure of SnS_2 consists of tin cations sandwiched between two layers of hexagonal closed pack (hcp) sulfur anions through weak van der Waals force between the layers; however, the strong force is present in the layer through in-plane covalent bonding [25]. The tin cations are coordinated octahedrally with six nearest neighbor sulfur anions. Different synthesis techniques are followed to synthesize SnS_2 material, such as solvothermal, hydrothermal, lasing ablation methods, sonochemical [26-32], etc. Among these methods, the hydrothermal method is preferable because it is simpler, less harmful, environmentally benign, cost-effective, and large yield. SnS_2 nanomaterial is prepared in this article by a simple hydrothermal method, and the optical and structural properties are investigated and reported here.

2. Materials and Methods

Stannic chloride pentahydrate ($Sncl_4.5H_2O$) (Loba Chemie Pvt. Ltd.), DI water, thioacetamide (C_2H_5NS) (TAA) (Loba Chemie Pvt. Ltd), and ethanol were used as received for the synthesis of SnS_2 without any further purification. Tin disulfide (SnS_2) was synthesized by following the hydrothermal method as follows. In a typical synthesis (schematically shown in figure 1), 1.72 g of stannic chloride pentahydrate ($SnCl_4.5H_2O$) and 0.98g of thioacetamide (TAA) were added in 38 mL of DI water. It was then stirred for 5 hours on a magnetic stirrer at room temperature to get the clear homogeneous solution. The resulting solution was then put in a 50 mL Teflon-lined stainless steel autoclave. The autoclave was then heated to 180 °C and maintained for 12 hours. After heating, the autoclave was kept for cooling down naturally. The precipitate was then centrifuged with DI water, followed by ethanol three times each. After drying in a hot air oven at 80 °C for 6 hours, the final yellow product was obtained. The obtained product was then characterized through different optical and structural characterization techniques such as X-ray Diffractometer (XRD) (Xpert^3 MRD XL, Panalytical), UV Vis NIR Spectrophotometer (Agilent, Model: Cary 5000), Photoluminescence spectroscopy (Fluoromax-4C Spectrofluorometer, Horiba), Raman Spectroscopy (Make: Horiba Jobin Vyon, LabRam HR), FTIR (Bruker ALPHA II compact spectrophotometer).

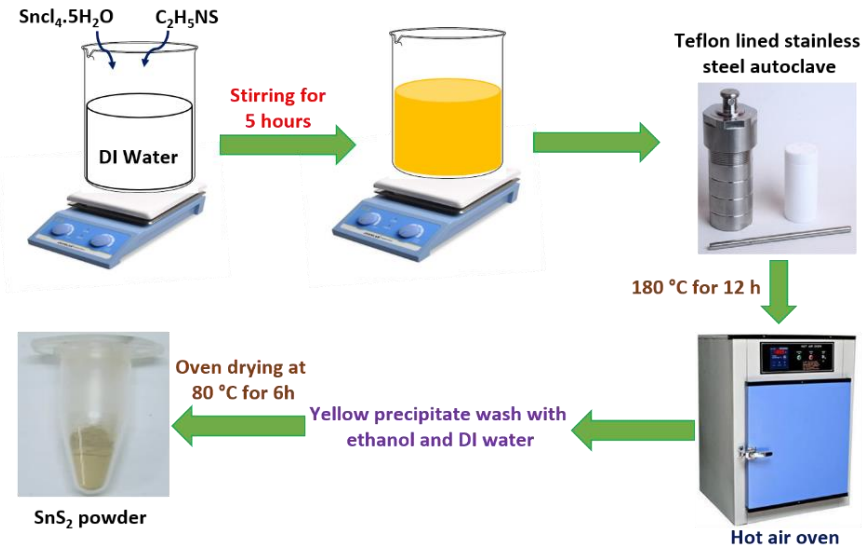

Figure 1. The schematic diagram for the synthesis of SnS_2.

In the synthesis procedure stannic chloride dissociates into Sn^{4+} ions and then reacts with H_2S that is produced during the hydrolysis process of thioacetamide to form SnS_2 ($CH_3CSNH_2 + 2H_2O = CH_3CO_2NH_4 + H_2S$; $2H_2S + Sn^{4+} = SnS_2 + 4H^+$).

3. Results and Discussion

3.1. Optical studies.

3.1.1. UV-visible DRS spectroscopy.

The UV-vis diffuse reflectance (DRS) spectra of SnS_2 are performed in the wavelength band of 200-800 nm, as displayed in figure 2(a). A broad hump appears at 340 nm, and also other three peaks are observed at 235, 295, and 395 nm, respectively, after deconvolution [33-35]. The optical band gap energies are estimated using Tauc's plot, and the values are found to be 2.14 and 4.02 eV, respectively, as shown in figure 2(b) using the formula $(\alpha h\nu)^n = A (h\nu - E_g)$ (where the absorption coefficient is represented by α, h corresponds to Plank constant, ν represents frequency, n corresponds to the type of transition, E_g represents band-gap, A is a constant).

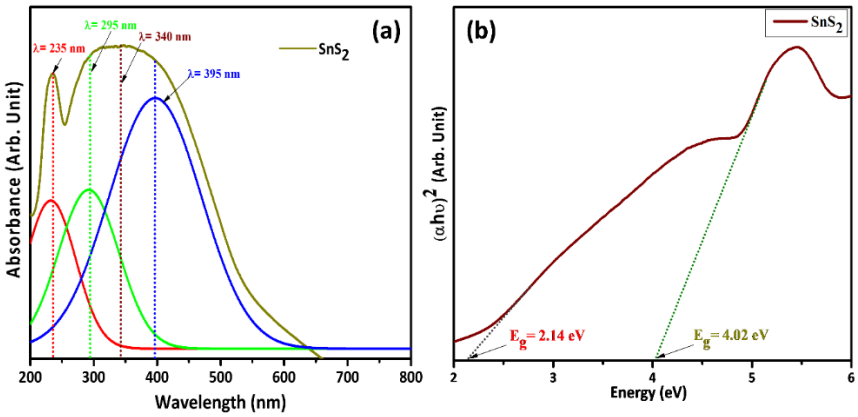

Figure 2. (a) UV-vis DRS spectroscopy of SnS_2; (b) Tauc's plot of SnS_2.

3.1.2. Photoluminescence (PL) spectroscopy.

The PL spectrum of SnS_2 is performed for the excitation wavelength 340 nm (λ_{ex} = 340 nm), as shown in figure 3. It is related to the emission of photons and the recombination of electron-hole. The PL spectrum shows a sharp emission peak at 561 nm, possibly because of the radiative recombination of bound excitons [36-39].

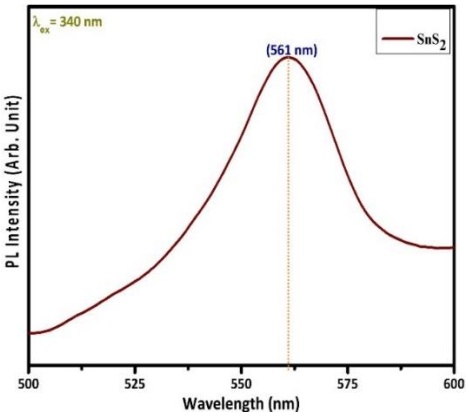

Figure 3. PL spectroscopy of SnS_2.

3.1.3. FTIR spectroscopy.

FTIR analysis of SnS_2 is performed in the wavenumber region of 4000-500 cm^{-1}, as shown in figure 4. It is performed to examine various functional groups in the material. The peak observes at 3410 cm^{-1} represents the vibration of the O-H bond. A peak at 625 cm^{-1} represents the Sn-S stretching vibration. The peak observes at 1711 cm^{-1} represents the existence of the carboxylic group [40-43].

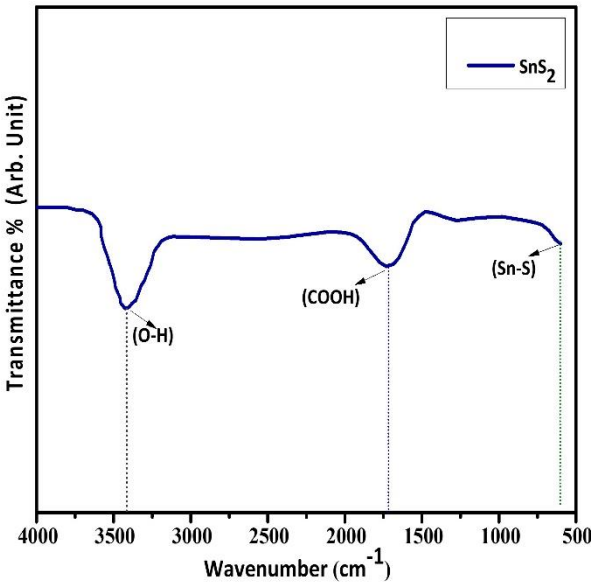

Figure 4. FTIR spectra of SnS_2.

3.1.4. Raman spectroscopy.

Raman spectra of SnS_2 nanocrystal are displayed in figure 5. The peak at 314 cm^{-1} represents A_{1g} mode of SnS_2, which occurs due to the out-of-plane vibration of sulfur atoms that signifies the presence of SnS_2 [44]. Another small peak observed at 206 cm^{-1} represents Eg mode, which is very weak and occurs due to plane stretching vibration [44,45].

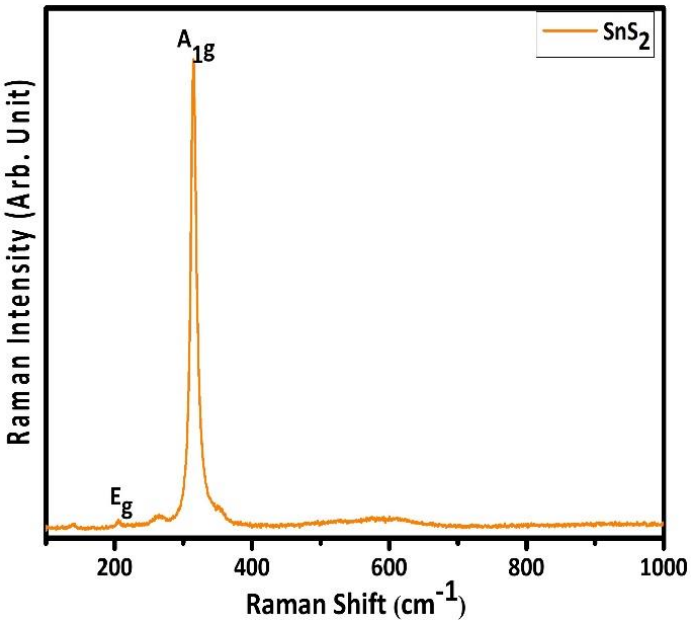

Figure 5. Raman spectra of SnS_2.

3.2. Structural analysis of SnS_2.

3.2.1. X-ray Diffraction (XRD).

The structural phase and interplanar spacing of SnS_2 are calculated using XRD analysis as shown in figure 6. It is performed in the 2θ range of 5° to 80° with CuK_α source with a wavelength of radiation λ =1.54Å. Different peaks are observed at 15.17°, 28.52°, 30.42°, 32.41°, 42.13°, 46.31°, 50.29°, 52.66°, 55.15°, 58.78°, 59.77°, 60.91°, 63.14°, 67.59°, 70.63°, and 77.71° which corresponds to (001), (100), (002), (101), (102), (003), (110), (111), (103), (200), (112), (201), (004), (202), (113), (203) planes, respectively [40,42,46-48]. These diffraction peaks confirm the hexagonal crystal structure of the material. Bragg's law 2d sinθ = nλ is used to determine the interplanar spacing of the material (where, n=1, d, and θ represent interplanar spacing and Bragg angle, respectively, and λ is the wavelength of X-ray) and is found to be 5.83 Å. Scherrer's formula is used to determine average crystallite size, $D = \frac{k\lambda}{\beta cos\theta}$ (where λ and β represent the X-ray wavelength and full-width half maxima, respectively. k is Scherrer constant (0.90), and θ is peak position in radian) and is found to be 28 nm. From W-H plot, the strain of the material is calculated, which is equal to -0.00011 (Negative value represents the compressive strain in the material), and also the average crystallite size is estimated to be 28 nm which is comparable with the crystallite size (27.68 nm) that is calculated from Scherrer's formula.

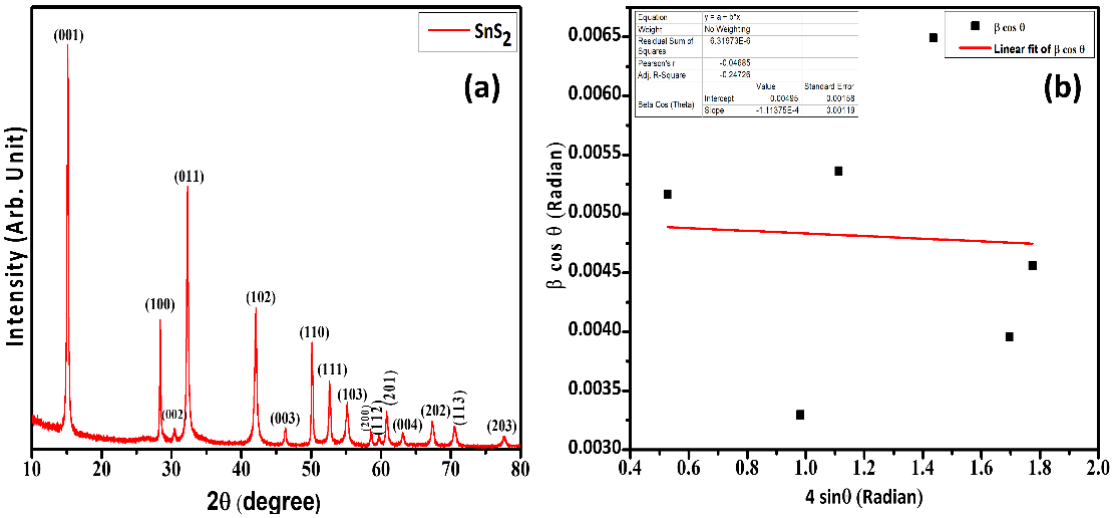

Figure 6. (a) XRD pattern of SnS_2; (b)WilliamsonHall (W-H) plot of SnS_2.

4. Conclusions

In this article, we follow a simple, environmentally benign, and cost-effective hydrothermal method to prepare SnS_2. The optical and structural investigations have been done for the synthesized material. Raman spectra depict the A_{1g} mode of vibration that occurs due to of plane vibration of sulfur atoms. PL emission spectra and UV-visible absorption spectra reveal electrons' emission and excitonic absorption in the material. An absorption peak near 625 cm^{-1} represents the existence of Sn-S vibration. The presence of different diffraction peaks suggests the hexagonal crystal structure of the material. Realization of better optical and structural behavior of the material can have found many exploitations in electronic and optoelectronic devices in coming years.

Funding

This research received no external funding.

Acknowledgments

The authors would like to thank CIF, NIT Silchar, DST-FIST (No. SR/FST/PSI-212/2016(C)) NIT Silchar, CIF IIT Guwahati.

Conflicts of Interest

The authors declare no conflict of interest.

References

1. Gajendiran, J.; Rajendran, V. Synthesis of SnS_2 nanoparticles by a surfactant-mediated hydrothermal method and their characterization. *Advances in Natural Sciences: Nanoscience and Nanotechnology* **2011**, *2*, http://doi.org/10.1088/2043-6262/2/1/015001.
2. Kane, R.S.; Cohen, R.E.; Silbey, R. Synthesis of PbS Nanoclusters within Block Copolymer Nanoreactors. *Chemistry of Materials* **1996**, *8*, 1919-1924, https://doi.org/10.1021/cm960072i.
3. Xia, X.; Zhu, C.; Luo, J.; Zeng, Z.; Guan, C.; Ng, C.F.; Zhang, H.; Fan, H.J. Synthesis of Free-Standing Metal Sulfide Nanoarrays via Anion Exchange Reaction and Their Electrochemical Energy Storage Application. *Small* **2014**, *10*, 766-773, https://doi.org/10.1002/smll.201302224.
4. Lai, C.-H.; Lu, M.-Y.; Chen, L.-J. Metal sulfide nanostructures: synthesis, properties and applications in energy conversion and storage. *Journal of Materials Chemistry* **2012**, *22*, 19-30, https://doi.org/10.1039/C1JM13879K.
5. Gaur, R.; Jeevanandam, P. Synthesis of SnS2 Nanoparticles and Their Application as Photocatalysts for the Reduction of Cr(VI). *Journal of Nanoscience and Nanotechnology* **2018**, *18*, 165-177, https://doi.org/10.1166/jnn.2018.14604.
6. Voznyi, A.; Kosyak, V.; Opanasyuk, A.; Tirkusova, N.; Grase, L.; Medvids, A.; Mezinskis, G. Structural and electrical properties of SnS2 thin films. *Materials Chemistry and Physics* **2016**, *173*, 52-61, https://doi.org/10.1016/j.matchemphys.2016.01.036.
7. Lin, L.; Chen, Y.; Tao, H.; Yao, L.; Huang, J.; Zhu, L.; Lou, M.; Chen, R.; Yan, L.; Zhang, Z. Ferromagnetism and optical properties of SnS2 doped with two impurities: first-principles calculations. *Physical Chemistry Chemical Physics* **2021**, *23*, 6574-6582, https://doi.org/10.1039/d0cp06322c.
8. Ali, A.; Zhang, J.-M.; Muhammad, I.; Shahid, I.; Ahmad, I.; Rehman, M.U.; Ahmad, I.; Kabir, F. First-principles investigation on electronic structure, magnetic states and optical properties of Mn-doped SnS2 monolayer via strain engineering. *Physica E: Low-dimensional Systems and Nanostructures* **2021**, *134*, https://doi.org/10.1016/j.physe.2021.114842.
9. Zhao, X.; Wang, M.; Niu, W.; Zhang, H.; Wang, T.; Dai, X. Tunable band alignments and optical properties in vertical heterojunctions of SnS2 and MoSe2. *Solid State Communications* **2021**, *323*, https://doi.org/10.1016/j.ssc.2020.114103.
10. Lin, L.; Lou, M.; Li, S.; Cai, X.; Zhang, Z.; Tao, H. Tuning electronic and optical properties of two–dimensional vertical van der waals arsenene/SnS2 heterostructure by strain and electric field. *Applied Surface Science* **2022**, *572*, https://doi.org/10.1016/j.apsusc.2021.151209.
11. Rusu, E.V.; Syrbu, N.N.; Tiron, A.V.; Zalamai, V.V. Band structure and optical constants of SnS2 single crystals. *Materials Research Express* **2019**, *6*, https://doi.org/10.1088/2053-1591/aafb25.
12. Domingo, G.; Itoga, R.S.; Kannewurf, C.R. Fundamental optical absorption of SnS2 and SnSe2. *Phys. Rev.* **1966**, *143*, 536-541, https://doi.org/10.1103/PhysRev.143.536.
13. Kherchachi, I.B.; Attaf, A.; Saidi, H.; Bouhdjer, A.; Bendjedidi, H.; Benkhetta, Y.; Azizi, R. Structural, optical and electrical properties of SnxSythin films grown by spray ultrasonic. *Journal of Semiconductors* **2016**, *37*, https://doi.org/10.1088/1674-4926/37/3/032001.
14. Arulanantham, A.M.S.; Valanarasu, S.; Kathalingam, A.; Shkir, M.; Kim, H.-S. An investigation on SnS layers for solar cells fabrication with CdS, SnS2 and ZnO window layers prepared by nebulizer spray method. *Applied Physics A* **2018**, *124*, https://doi.org/10.1007/s00339-018-2164-6.
15. Morales, J.; Vicente, C.P.; Santos, J.; Tirado, J.L. Electrochemical Characteristics of Crystalline and Amorphous SnS2 in Lithium Cells. *Journal of The Electrochemical Society* **1996**, *143*, 2847-2851, https://doi.org/10.1149/1.1837117.
16. Mishra, R.K.; Choi, G.J.; Mishra, Y.K.; Kaushik, A.; Sohn, Y.; Lee, S.H.; Gwag, J.S. A highly stable, selective, and high-performance VOC sensor using a SnS2 nano-lotus structure. *Journal of Materials Chemistry C* **2021**, *9*, 7713-7725, https://doi.org/10.1039/D1TC00615K.

17. Chen, X.; Jiang, H.; Pei, Y.; Chen, Y.; Zeng, Y.; Guo, H. Binder-free ultrathin SnS2 with superior reversibility of conversion reaction for high-rate lithium ion batteries. *Journal of Alloys and Compounds* **2021**, *873*, https://doi.org/10.1016/j.jallcom.2021.159623.
18. Ermolaev, G.A.; Yakubovsky, D.I.; El-Sayed, M.A.; Tatmyshevskiy, M.K.; Mazitov, A.B.; Popkova, A.A.; Antropov, I.M.; Bessonov, V.O.; Slavich, A.S.; Tselikov, G.I.; Kruglov, I.A.; Novikov, S.M.; Vyshnevyy, A.A.; Fedyanin, A.A.; Arsenin, A.V.; Volkov, V.S. Broadband Optical Constants and Nonlinear Properties of SnS2 and SnSe2. *Nanomaterials* **2022**, *12*, https://doi.org/10.3390/nano12010141.
19. Ahmed, H.; Hashim, A. Design and Tailoring the Optical and Electronic Characteristics of Silicon Doped PS/SnS2 New Composites for Nano-Semiconductors Devices. *Silicon* **2021**, *13*, https://doi.org/10.1007/s12633-021-01449-x.
20. Roshan, H.; Salimi Kuchi, P.; Sheikhi, M.H.; Mirzaei, A. Enhancement of room temperature ethanol sensing behavior of PbS–SnS2 nanocomposite by Au decoration. *Materials Science in Semiconductor Processing* **2021**, *127*, https://doi.org/10.1016/j.mssp.2021.105742.
21. He, C.-J.; Wang, Y.-Q.; Meng, W.-J.; Zhang, J.; Xie, Y.; Hou, Y.-L.; Zhao, D.-L. Hierarchical microspheres constructed by SnS2 nanosheets and S-doped graphene for high performance lithium/sodium-ion batteries. *Journal of Alloys and Compounds* **2021**, *889*, https://doi.org/10.1016/j.jallcom.2021.161648.
22. Tripathi, S.; Kumar, B.; Dwivedi, D.K. Numerical simulation of non-toxic In2S3/SnS2 buffer layer to enhance CZTS solar cells efficiency by optimizing device parameters. *Optik* **2021**, *227*, https://doi.org/10.1016/j.ijleo.2020.166087.
23. Su, X.; Su, D.; Sang, Z.; Yan, X.; Liang, J. Shielded SnS2/SnS heterostructures on three-dimensional graphene framework for high-rate and stable sodium-ion storage. *Electrochimica Acta* **2021**, *372*, http://dx.doi.org/10.1016/j.electacta.2021.137800.
24. Guan, Y.; Li, X.; Hu, T.; Zhang, N.; Niu, R.; Liu, Z. Tunable electronic properties of SnS2/WSe2 hetero-structure: A frist principle study. *Superlattices and Microstructures* **2021**, *150*, https://doi.org/10.1016/j.spmi.2021.106806.
25. Fan, C.; Li, Y.; Lu, F.; Deng, H.-X.; Wei, Z.; Li, J. Wavelength dependent UV-Vis photodetectors from SnS2 flakes. *RSC Advances* **2016**, *6*, 422-427, https://doi.org/10.1039/C5RA24905H.
26. Hong, S.Y.; Popovitz-Biro, R.; Prior, Y.; Tenne, R. Synthesis of SnS2/SnS Fullerene-like Nanoparticles: A Superlattice with Polyhedral Shape. *Journal of the American Chemical Society* **2003**, *125*, 10470-10474, https://doi.org/10.1021/ja036057d.
27. Hai, B.; Tang, K.; Wang, C.; An, C.; Yang, Q.; Shen, G.; Qian, Y. Synthesis of SnS2 nanocrystals via a solvothermal process. *Journal of Crystal Growth* **2001**, *225*, 92-95, https://doi.org/10.1016/S0022-0248(01)01030-2.
28. Chen, D.; Shen, G.Z.; Tang, K.B.; Liu, Y.K.; Qian, Y.T. Aligned SnS2 nanotubes fabricated via a template-assisted solvent-relief process. *Applied Physics A* **2003**, *77*, 747-749, https://doi.org/10.1007/s00339-003-2215-4.
29. Yang, Q.; Tang, K.; Wang, C.; Zhang, D.; Qian, Y. The Synthesis of SnS2 Nanoflakes from Tetrabutyltin Precursor. *Journal of Solid State Chemistry* **2002**, *164*, 106-109, https://doi.org/10.1006/jssc.2001.9453.
30. Johny, J.; Guzman, S.S.; Krishnan, B.; Martinez, J.A.A.; Avellaneda Avellaneda, D.; Shaji, S. SnS2 nanoparticles by liquid phase laser ablation: Effects of laser fluence, temperature and post irradiation on morphology and hydrogen evolution reaction. *Applied Surface Science* **2019**, *470*, 276-288, https://doi.org/10.1016/j.apsusc.2018.11.157.
31. Johny, J.; Sepulveda-Guzman, S.; Krishnan, B.; Avellaneda, D.; Shaji, S. Facile and fast synthesis of SnS2 nanoparticles by pulsed laser ablation in liquid. *Applied Surface Science* **2018**, *435*, 1285-1295, https://doi.org/10.1016/j.apsusc.2017.11.243.
32. Matyszczak, G.; Jóźwik, P.; Polesiak, E.; Sobieska, M.; Krawczyk, K.; Jastrzębski, C.; Płociński, T. Sonochemical preparation of SnS and SnS2 nano- and micropowders and their characterization. *Ultrasonics Sonochemistry* **2021**, *75*, https://doi.org/10.1016/j.ultsonch.2021.105594.
33. Kim, K.M.; Kwak, B.S.; Kang, S.; Kang, M. Synthesis of submicron hexagonal plate-type SnS2 and band gap tuned Sn1-xTixS2 materials and their hydrogen production abilities on methanol/water photosplitting. *International Journal of Photoenergy* **2014**, *2014*, 1-9, https://doi.org/10.1155/2014/479508.
34. Chen, C.; Xun, L.; Zhang, P.; Zhang, J.; Tian, B. Z-scheme structure SnS2–Au–CdS with excellent photocatalytic performance for simultaneous removal of Cr(VI) and methyl orange. *Research on Chemical Intermediates* **2019**, *45*, 3513-3524, https://doi.org/10.1007/s11164-019-03805-4.
35. Wu, X.-F.; Li, H.; Sun, Y.; Wang, Y.-J.; Zhang, C.-X.; Su, J.-Z.; Zhang, J.-R.; Yang, F.-F.; Zhang, Y.; Pan, J.-C. Synthesis of SnS2/few layer boron nitride nanosheets composites as a novel material for visible-light-driven photocatalysis. *Applied Physics A* **2017**, *123*, https://doi.org/10.1007/s00339-017-1286-6.
36. Kaur, J.; Sunaina; Zaidi, Z.; Vaidya, S. New synthetic methodology to enhance Mg doping in SnS2: structural characterization and photocatalytic activity. *Bulletin of Materials Science* **2020**, *43*, https://doi.org/10.1007/s12034-020-02280-7.
37. Arulanantham, A.M.S.; Valanarasu, S.; Kathalingam, A.; Jeyadheepan, K. Influence of carrier gas pressure on nebulizer spray deposited tin disulfide thin films. *Journal of Materials Science: Materials in Electronics* **2018**, *29*, 11358-11366, https://doi.org/10.1007/s10854-018-9223-9.

38. Deshpande, N.G.; Sagade, A.A.; Gudage, Y.G.; Lokhande, C.D.; Sharma, R. Growth and characterization of tin disulfide (SnS2) thin film deposited by successive ionic layer adsorption and reaction (SILAR) technique. *Journal of Alloys and Compounds* **2007**, *436*, 421-426, https://doi.org/10.1016/j.jallcom.2006.12.108.
39. Ham, G.; Shin, S.; Park, J.; Lee, J.; Choi, H.; Lee, S.; Jeon, H. Engineering the crystallinity of tin disulfide deposited at low temperatures. *RSC Advances* **2016**, *6*, 54069-54075, https://doi.org/10.1039/C6RA08169J.
40. Joseph, A.; Anjitha, C.R.; Aravind, A.; Aneesh, P.M. Structural, optical and magnetic properties of SnS2 nanoparticles and photo response characteristics of p-Si/n-SnS2 heterojunction diode. *Applied Surface Science* **2020**, *528*, https://doi.org/10.1016/j.apsusc.2020.146977.
41. Wei, R.; Zhou, R.; Hu, J.; Li, J. Glutatione modified ultrathin SnS2 nanosheets with highly photocatalytic activity for wastewater treatment. *Mater. Res. Express.* **2014**, *1*.
42. Duangchuen, T.; Karaphun, A.; Wannasen, L.; Kotutha, I.; Swatsitang, E. Effect of SnS2 concentrations on electrochemical properties of SnS2/RGO nanocomposites synthesized by a one-pot hydrothermal method. *Applied Surface Science* **2019**, *487*, 634-646, https://doi.org/10.1016/j.apsusc.2019.05.116.
43. Liu, H.; Du, C.; Bai, H.; Su, Y.; Wei, D.; Wang, Y.; Liu, G.; Yang, L. Fabrication of plate-on-plate Z-scheme SnS2/Bi2MoO6 heterojunction photocatalysts with enhanced photocatalytic activity. *Journal of Materials Science* **2018**, *53*, 10743-10757, https://doi.org/10.1007/s10853-018-2296-2.
44. Burton, L.A.; Whittles, T.J.; Hesp, D.; Linhart, W.M.; Skelton, J.M.; Hou, B.; Webster, R.F.; O'Dowd, G.; Reece, C.; Cherns, D.; Fermin, D.J.; Veal, T.D.; Dhanak, V.R.; Walsh, A. Electronic and optical properties of single crystal SnS2: an earth-abundant disulfide photocatalyst. *Journal of Materials Chemistry A* **2016**, *4*, 1312-1318, https://doi.org/10.1039/C5TA08214E.
45. Gurnani, C.; Hawken, S.L.; Hector, A.L.; Huang, R.; Jura, M.; Levason, W.; Perkins, J.; Reid, G.; Stenning, G.B.G. Tin(iv) chalcogenoether complexes as single source precursors for the chemical vapour deposition of SnE_2 and SnE (E = S, Se) thin films. *Dalton Transactions* **2018**, *47*, 2628-2637, https://doi.org/10.1039/C7DT03848H.
46. Li, M.; Liu, E.; Hu, H.; Ouyang, S.; Xu, H.; Wang, D. Surfactant-free synthesis of single crystalline SnS2 and effect of surface atomic structure on the photocatalytic property. *Journal of Photoenergy* **2014**, *2014*, 1-7, https://doi.org/10.1155/2014/394146.
47. Anlin Lazar, K.; Cicily Rigi, V.J.; Divya, D.; Saji, K.J. Effect of annealing on structural and optical properties of SnS2 thin films grown by thermal evaporation and post sulphur annealing technique. *IOP Conference Series: Materials Science and Engineering* **2021**, *1166*, https://doi.org/10.1088/1757-899X/1166/1/012004.
48. Joseph, A.; Aneesh, P.M. Efficient degradation of methylene blue: A comparative study using hydrothermally synthesised SnS_2, WS_2 and VS_2 nanostructures. *Materials Research Bulletin* **2022**, *146*, https://doi.org/10.1016/j.materresbull.2021.111623.